Control of Aeroelastic Instabilities Through Stiffness Cross-Coupling

Terrence A. Weisshaar*
Purdue University, West Lafayette, Indiana
and
Rosemary J. Ryan†
Rockwell International Corporation, Los Angeles, California

An idealized aeroelastic tailoring model is developed to assess the effects of significant changes in directional stiffness orientation upon the flutter and divergence behavior of swept and unswept wings. A nondimensional stiffness cross-coupling parameter is used to illustrate the potentially strong influence of stiffness cross-coupling, commonly present in aeroelastically tailored structures, to increase flutter and divergence speeds. Conflicting requirements for flutter and divergence enhancement are indicated. Aeroelastic tailoring for flutter enhancement appears to be less effective when the wing is moderately swept back. However, by combining directional stiffness orientation with inertia balancing, flutter and divergence-free, aft-swept, high-aspect-ratio surfaces are shown to be theoretically possible.

Introduction

THE term "aeroelastic tailoring" is used to describe a portion of the aircraft design process that considers the effects of directional stiffness orientation to control aeroelastic deformation, either static or dynamic. Aeroelastic tailoring may be used to modify a number of aspects of aircraft performance such as lift-to-drag ratio, lift effectiveness, control effectiveness, and structural stability, e.g., flutter and divergence. While not restricted to laminated composite construction, aeroelastic tailoring nonetheless finds its greatest potential when applied to this type of structural construction.

Aeroelastic tailoring is, in fact, a structural optimization procedure with aeroelastic objectives and constraints used to choose laminate thickness distributions and ply orientations for lifting surfaces. Reference 1 discusses a number of ad hoc examples of the use of aeroelastic tailoring to produce flutter and divergence enhancement. No single "tailoring parameter" is used in these studies, making it difficult to assess the consequences of introducing stiffness cross-coupling into a lifting surface design. The present study has two objectives: 1) the development of an idealized aeroelastic model suitable for parameter studies encompassing a wide range of potential designs, and 2) the illustration of the potential effects of tailoring when applied to flutter and divergence enhancement.

For moderate-to-high aspect-ratio surfaces, aeroelastic tailoring effectiveness relies upon the interaction or coupling between shear strain and normal strains such as might be found in an anisotropic laminate (or an orthotropic laminate rotated with respect to some reference axis). Such normal/shear strain coupling leads to coupling between bending deformation and twisting rotation about a reference axis when loads are applied along this axis. Equivalent plate or beam theory models are available for analytical predictions of tailoring effects. When displayed on graphs or charts the effects of parameter changes are apparent for the design in question.

Despite the availability of sophisticated methods, problems remain. For instance, it is not clear how to choose a characteristic, bounded parameter that may be used to assess the full range of design possibilities. For instance, if a benefit is identified for a specific planform, can it be extended to similar planforms? What, if any, are the limitations of aeroelastic tailoring? This paper will examine these questions by approaching divergence and flutter as mechanical instabilities whose underlying cause is the aeroelastic interaction between characteristic deformations of the lifting surface. A simplified idealization is used to survey aeroelastic stability trends for selected configurations as a function of significant design parameters such as wing sweep, inertia placement, and a nondimensional stiffness cross-coupling parameter. Significant trends, features, and limitations of tailoring are then identified. Where possible, results of this study will be correlated with results from other, more sophisticated studies.

Model Development

The workhorse of all aeroelastic models is the two-dimensional, "typical section" (see, for instance, Ref. 2) used for unswept wing flutter analysis. This idealization traces its origins to the 1930s; it is still used extensively, both in educational and research efforts, such as the study of transonic aeroelasticity. The advantages of such models are twofold. Algebraic expressions for the equations of motion of such idealizations reveal a great deal about potential inertial, structural, and aerodynamic interactions. In addition, for certain extreme cases, closed-form solutions for flutter and divergence speeds may be found.

A two-degree-of-freedom model of a swept lifting surface has also been used to study static stability of swept wings.[3] Certain desirable features of this latter model suggested the idealization chosen for the present study. Consider the planform, similar to that used in Ref. 3, shown in Fig. 1. The surface itself is rigid with mass uniformly distributed along the span. A reference axis, denoted as the y axis in Fig. 1b, originates at a pivot fixed in space, and is used to describe air-

Presented as Paper 84-0985 at the AIAA/ASME/ASCE/AHS 25th Structures, Structural Dynamics and Materials Conference, Palm Springs, CA, May 14-16, 1984; received July 7, 1984; revision received July 25, 1985.

*Professor, School of Aeronautics and Astronautics. Associate Fellow AIAA.
†Engineer. Member AIAA.

foil deflection in terms of the rotation angles θ and ϕ; this axis is swept at an angle Λ to the freestream. The offset of the line of aerodynamic centers used for static analysis (located at the ¼ chord) and this y axis is denoted as e in Fig. 1c. The offset of the line of centers of mass and the reference axis is denoted as x_α; this latter parameter is positive when the sectional centers of mass are located aft of the reference axis. The chordwise dimension c and spanwise dimension ℓ determine the planform area $S=\ell c$ and the structural aspect ratio $\ell/c=\bar{R}$.

Unlike Ref. 3, the model shown in Fig. 1b has principal stiffness axes oriented at angles γ and $(\gamma+90$ deg) with respect to the y axis. K_θ is a torsion spring constant associated with twisting about an axis oriented at an angle γ with respect to y in Fig. 1b. Similarly, K_ϕ is associated with rotation about an axis normal to the y axis in Fig. 1b; this spring is the "bending" spring. This K_θ, K_ϕ combination is intended to simulate the effect of an orthotropic laminate as it is rotated in the plane of the wing.

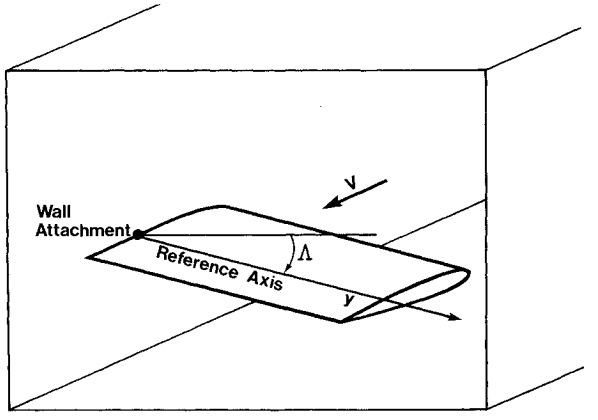

Fig. 1 a) Semirigid airfoil shown swept at an angle Λ to the airstream and attached to a fixed pivot.

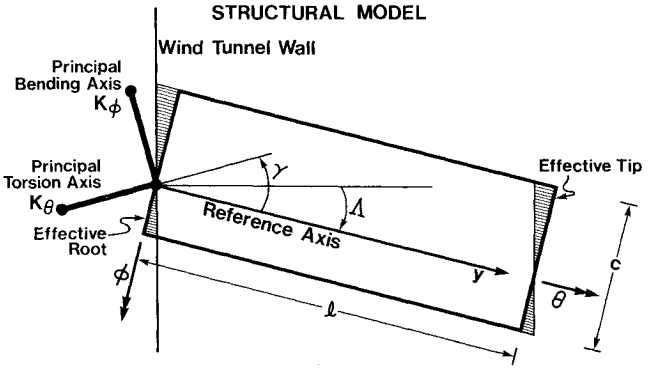

Fig. 1 b) Planform view showing rotational deformations θ and ϕ, orientation of principal bending and torsion axes γ, and effective root and tip approximations.

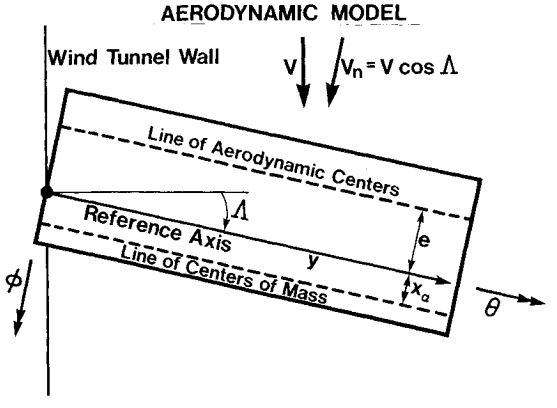

Fig. 1 c) Planform view showing aerodynamic center/reference axis offset, reference axis/center-of-mass offset, and normal component of velocity V_n.

A two-dimensional, quasisteady airload approximation that neglects the effects of the airfoil wake and damping was used in this development. Neglect of damping may not be serious if the fluid density is low in comparison to that of the wing. Airloads acting perpendicular to the y axis in Fig. 1c are defined and then used to compute aerodynamic moments about spanwise and chordwise axes located at the pivot. These loads are expressed in terms of the the deflection coordinates θ and ϕ and are denoted as M_θ and M_ϕ.

$$\begin{Bmatrix} M_\theta \\ M_\phi \end{Bmatrix} = qSC_{L_\alpha}\cos^2\Lambda \begin{bmatrix} e & -e\tan\Lambda \\ y_{cp} & -y_{cp}\tan\Lambda \end{bmatrix} \begin{Bmatrix} \theta \\ \phi \end{Bmatrix} \equiv [A_{ij}] \begin{Bmatrix} \theta \\ \phi \end{Bmatrix} \tag{1}$$

The coordinate y_{cp} measures the spanwise center-of-pressure position, with respect to the root support, measured along the y axis.

The equations of motion for free vibration of this semirigid swept-wing model are written symbolically as

$$[M_{ij}]\begin{Bmatrix} \ddot{\theta} \\ \ddot{\phi} \end{Bmatrix} + [K_{ij}]\begin{Bmatrix} \theta \\ \phi \end{Bmatrix} + [A_{ij}]\begin{Bmatrix} \theta \\ \phi \end{Bmatrix} = \begin{Bmatrix} 0 \\ 0 \end{Bmatrix}, \quad i,j=1,2 \tag{2}$$

The inertia terms are

$$M_{11} = m(r_0^2 + x_\alpha^2) = mr_\alpha^2 \tag{3}$$

$$M_{12} = -mx_\alpha \ell/2 \tag{4}$$

$$M_{22} = m\ell^2/3 \tag{5}$$

where m is the total mass of the wing and r_0 the radius of gyration of the wing about the line of centers of mass parallel to the y axis. The factor of 3 in Eq. (5) reflects the uniformity of the mass distribution along the span.

In terms of the angle γ and spring constants K_θ and K_ϕ, the stiffness terms in Eq. (2) are

$$K_{11} = K_\theta\cos^2\gamma + K_\phi\sin^2\gamma \tag{6}$$

$$K_{12} = (K_\phi - K_\theta)\sin\gamma\cos\gamma \tag{7}$$

$$K_{22} = K_\theta\sin^2\gamma + K_\phi\cos^2\gamma \tag{8}$$

The presence of the term K_{12} when γ is nonzero produces an effect known as "stiffness cross-coupling." The determinant of the stiffness matrix is written as follows:

$$\Delta = K_{11}K_{22}\left[1 - \frac{K_{12}^2}{K_{11}K_{22}}\right] \tag{9}$$

The condition that the stiffness matrix be positive definite results in the following requirement:

$$\frac{K_{12}^2}{K_{11}K_{22}} < 1 \tag{10}$$

Because of Eq. (10), a nondimensional stiffness cross-coupling parameter ψ may defined as follows:

$$\psi = \frac{-K_{12}}{\sqrt{K_{11}K_{22}}}, \quad -1 < \psi < 1 \tag{11}$$

The minus sign is included in Eq. (11) so that positive ψ values indicate that upward "bending" $(+\phi)$ is accompanied by nose-up "twist" $(+\theta)$. Positive values of ψ will lead to a "wash-in" wing (bend up/twist up), while negative values lead to a "wash-out" (bend up/twist down) wing.

An additional stiffness parameter is present and defined as

$$R = K_{11}/K_{22} \tag{12}$$

This parameter, referenced to the y axis, defines the ratio of "torsional" to "bending" stiffness and is called the "primary stiffness ratio."

If the spring-stiffness values K_ϕ and K_θ are fixed while γ is changed, K_{11}, K_{22}, and K_{12} change simultaneously. However, a primary objective here is the examination of independent changes in R and ψ. Three parameters, K_{11} (which represents torsional stiffness measured about the y axis), R, and ψ can be used to describe the stiffness characteristics of this model. For a laminated structure such parameters are controlled by ply orientation and laminate construction, while in the present case they are controlled by structural axis orientation γ and spring stiffnesses K_ϕ and K_θ.

When the equations of motion represented in Eq. (2) are nondimensionalized, a number of familiar nondimensional aeroelastic, inertial, and structural parameters appear. To solve these nondimensional, time-dependent equations, motion is assumed to be of the form

$$\begin{Bmatrix} \theta \\ \phi \end{Bmatrix} = \begin{Bmatrix} \bar{\theta} \\ \bar{\phi} \end{Bmatrix} e^{st} \tag{13}$$

As a result, the equations of motion for vibration of the airfoil in the presence of the airstream may be written as

$$\begin{bmatrix} (\bar{s}^2+1) & \left(\bar{s}^2\left[\frac{-\bar{x}_\alpha \bar{\mathcal{R}}}{2\bar{r}_\alpha^2}\right]-\frac{\psi}{\sqrt{R}}\right) \\ \left(\bar{s}^2\left[\frac{-\bar{x}_\alpha \bar{\mathcal{R}}}{2\bar{r}_\alpha^2}\right]-\frac{\psi}{\sqrt{R}}\right) & \left(\frac{\bar{s}^2\bar{\mathcal{R}}^2}{3\bar{r}_\alpha^2}+\frac{1}{R}\right) \end{bmatrix} \begin{Bmatrix} \bar{\theta} \\ \bar{\phi} \end{Bmatrix}$$

$$+\frac{1}{2}\left(\frac{(\bar{V}\cos\Lambda)^2 C_{L_\alpha}}{\pi\mu\bar{r}_\alpha^2}\right)\begin{bmatrix} -\bar{e} & \bar{e}\tan\Lambda \\ \bar{y}\bar{\mathcal{R}} & \bar{y}\bar{\mathcal{R}}\tan\Lambda \end{bmatrix}\begin{Bmatrix} \bar{\theta} \\ \bar{\phi} \end{Bmatrix} = \begin{Bmatrix} 0 \\ 0 \end{Bmatrix} \tag{14}$$

In Eq. (14), $\bar{s}$ is defined as

$$\bar{s}^2 = s^2/\omega_p^2 \tag{15}$$

where reference frequency ω_p *is*

$$\omega_p^2 = K_{11}M_{11} \tag{16}$$

The reduced velocity $\bar{V}$ is defined as

$$\bar{V} = \frac{V}{\omega_p(c/2)} \tag{17}$$

The normal component of $\bar{V}$ is written as

$$\bar{V}_n = \bar{V}\cos\Lambda \tag{18}$$

The terms $\bar{x}_\alpha$, $\bar{e}$, and $\bar{r}\alpha$ refer to x_α, e, and r_α quantities nondimensionalized with respect to the chord, c. The term $\bar{y}$ is y_{cp}/ℓ.

The frequency determinant for Eq. (14) has the following form:

$$a\bar{s}^4 - b\bar{s}^2 - d\bar{V}_n^2\bar{s}^2 + f + \bar{V}_n^2 g = 0 \tag{19}$$

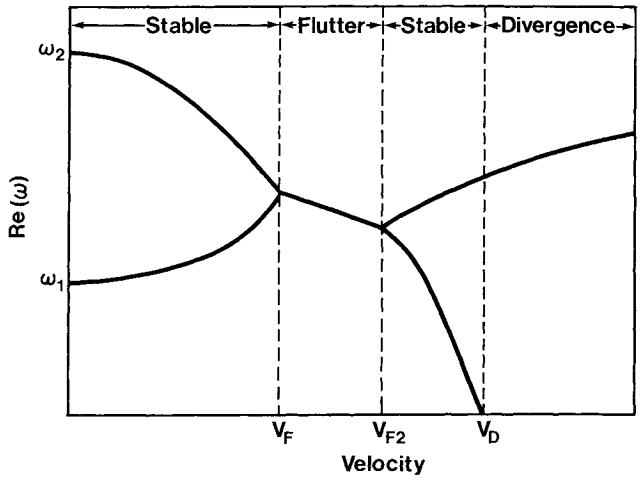

Fig. 2 Typical frequency vs airspeed behavior for the two-dimensional semirigid airfoil; ω is real when $V < V_F$ and is complex between V_F and V_{F2}.

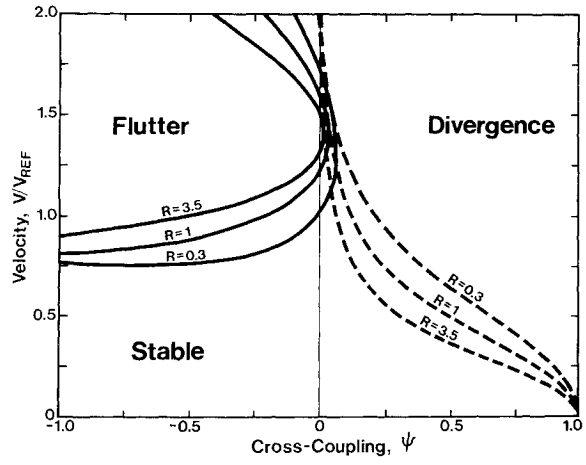

Fig. 3 Flutter and divergence speed boundaries as functions of R and ψ for an unswept wing (Table 1). Dashed line, divergence speed; solid lines, flutter.

where the coefficients a, b, d, f, and g are defined as

$$a = \frac{\bar{\mathcal{R}}^2}{3\bar{r}_\alpha^2}\left[\frac{\bar{r}_0^2 + \tfrac{1}{4}\bar{x}_\alpha^2}{\bar{r}_\alpha^2}\right] \tag{20}$$

$$b = -\frac{1}{R}\left[1 + \frac{R\bar{\mathcal{R}}^2}{3\bar{r}_\alpha^2} - \frac{\bar{x}_\alpha\bar{\mathcal{R}}\psi\sqrt{R}}{\bar{r}_\alpha^2}\right] \tag{21}$$

$$d = -\xi\bar{\mathcal{R}}\left[\bar{y}\tan\Lambda\frac{-\bar{\mathcal{R}}e}{3\bar{r}_\alpha^2} + \frac{\bar{x}_\alpha}{2\bar{r}_\alpha^2}(\bar{e}\tan\Lambda - \bar{y}\bar{\mathcal{R}}\right] \tag{22}$$

where

$$\xi = C_{L_\alpha}/2\pi^2\mu\bar{r}_\alpha^2 \tag{23}$$

$$f = (1-\psi^2)/R \tag{24}$$

$$g = \xi[-\bar{e} + R\,\bar{y}\bar{\mathcal{R}}\tan\Lambda + \psi\sqrt{R}(\bar{e}\tan\Lambda - \bar{y}\bar{\mathcal{R}})] \tag{25}$$

Reference 4 provides an in-depth discussion of the stability characteristics of a system with a characteristic equation of the form given by Eq. (19). First, note that at zero airspeed the system is conservative; the roots $\bar{s}$ will be complex with no real

part. With no damping, but with the aerodynamic stiffness terms included, the roots $\bar{s}$ will be purely imaginary for a range of airspeeds from zero up to a certain value. This implies that motion in the presence of the airstream is, at best, neutrally stable. Above a certain airspeed value, in this case, the flutter speed, the character of the roots $\bar{s}$ changes from purely imaginary to complex conjugate pairs. One of these conjugate pairs will have a real part greater than zero, implying that the amplitude of oscillatory motion is growing exponentially with time. Thus, the appearance of the conjugate pair signals instability. Because the character of the motion is purely sinusoidal up to the critical speed, it is more common to discuss the oscillatory behavior in terms of a frequency ω rather than s. To do this, set

$$\bar{s} = i\Omega \tag{26}$$

where $\Omega = \omega/\omega_p$. In terms of Ω, Eq. (19) becomes

$$a\Omega^4 + (b + \bar{V}_n^2 d)\Omega^2 + (f + \bar{V}_n^2 g) = 0 \tag{27}$$

Solving for Ω^2,

$$\Omega^2 = \{ -(b + \bar{V}_n^2 d \pm [(b + \bar{V}_n^2 d)^2 - 4a(f + \bar{V}_n^2 g)]^{1/2}\}/2a \tag{28}$$

Increasing airspeed may cause the two natural frequencies given in Eq. (28) to coalesce or "merge."[4] This phenomenon is illustrated conceptually in Fig. 2. Further increases in airspeed cause the radical in Eq. (28) to become complex. The onset of flutter occurs when the expression under the radical in Eq. (28) is zero. This occurs when

$$(b + \bar{V}_n^2 d)^2 = 4a(f + \bar{V}_n^2 g) \tag{29}$$

or

$$\bar{V}_F^2 = \frac{-(bd - 2ag) \pm 2[a(-bdg + ag^2 + d^2 f)]^{1/2}}{d^2(\cos^2\Lambda)} \tag{30}$$

From Eq. (30), two values of airspeed lead to frequency merging; Ω is complex between these two airspeeds, implying unstable motion. The lower airspeed is the flutter speed, denoted as V_F in Fig. 2. The higher speed, denoted as V_{F2}, is the speed at which the system regains stability; at this speed, the natural frequencies $\Omega_{1,2}$ again become real. This upper speed seldom is a physical reality.

The flutter speed, as given in Eq. (30), can become a complex number under two conditions; when this happens, flutter is not possible. Conceptually, this occurs when V_F and V_{F2} (see Fig. 2) merge so that no unstable region remains. This situation occurs when the radical in Eq. (30) is zero. Setting the terms under this radical equal to zero defines a condition at which system flutter will disappear. This yields a quadratic in the cross-coupling parameter ψ, implying that two values of ψ exist to cause flutter to disappear from the system. In addition, if the quantity $(bd - 2ag)$ in Eq. (30) is positive (see, for instance, Ref. 4, pp. 269-274) instability also is present.

Returning to Eq. (27), we see that one value of Ω^2 will be zero when

$$\bar{V}_n^2 = -f/g \tag{31}$$

This condition is also illustrated in Fig. 2 as the velocity labeled V_D. At airspeeds in excess of $\bar{V}_n^2 = -f/g$, a value of Ω obtained from Eq. (27) is purely imaginary, implying that the system is exponentially divergent (hence, the term "divergence") in time. Note that both f and g are functions of ψ so that the divergence speed can be controlled by ψ.

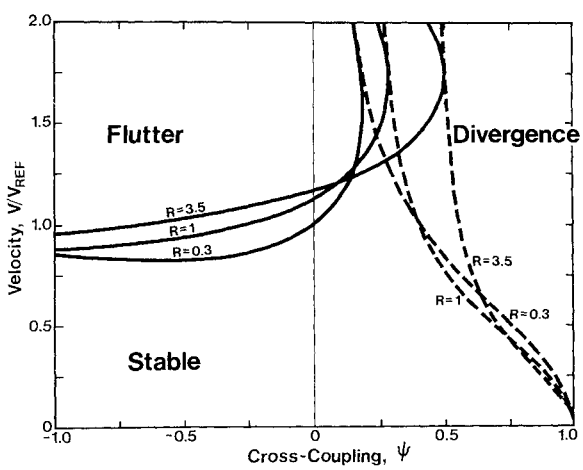

Fig. 4 Behavior of flutter and divergence speed boundaries as functions of R and ψ for the 15-deg sweptback wing; V_{ref} is unique to this sweep angle.

Tailoring Studies—An Example

To demonstrate some interesting features of aeroelastic tailoring, a fixed set of parameters was chosen as follows:

Table 1 Parameters for example wing

$\bar{e} = 0.10$	$C_{L_\alpha} = 4.0/\text{rad}$
$\bar{y} = 0.50$	$\mu = 10.0$
$\bar{x}_\alpha = 0.10$	$\ell/c = \bar{AR} = 4.0$
$\bar{r}_\alpha^2 = 0.25$	

The sweep angle Λ, stiffness ratio R, and cross-coupling parameter ψ are treated as independent design parameters.

First, consider the aeroelastic stability of an unswept wing. Three different values of the primary stiffness ratio R were considered ($R = 0.3$, 1.0, 3.5); K_{11} was fixed while ψ was allowed to vary from -1 to $+1$. Flutter and divergence boundaries were then obtained as a function of ψ. Results are shown in Fig. 3; dashed lines represent the locus of divergence speeds vs ψ at fixed R values. Note that these divergence speeds, shown in nondimensional form in Fig. 3, decline rapidly when ψ increases from zero. Furthermore, this decline is more pronounced when the primary stiffness ratio R is large (bending stiffness is small).

The divergence speed becomes infinite when ψ is less than a value denoted as ψ_D; this value is computed from Eq. (31) by setting $g = 0$. The result is

$$\psi_D = \frac{\bar{e} - R\bar{y}\bar{AR}\tan\Lambda}{\sqrt{R(\bar{e}\tan\Lambda - \bar{y}\bar{AR})}} \tag{32}$$

Note the dependence of ψ_D on R and Λ. At values of ψ less than ψ_D, $\bar{V}_n^2$ will be negative.

As shown in Fig. 3, the flutter speed (defined by the lower curve) declines when ψ decreases: however, flutter does not occur above certain values of ψ, denoted as ψ_{cr}. These special values of ψ are functions of R; when $\psi = \psi_{cr}$, the radical in Eq. (30) will vanish. Note that, with fixed values of K_{11} and ψ, a decrease in the primary stiffness ratio R results in lower flutter speeds if all other parameters remain fixed.

Sweeping the wing aft 15 deg modifies the influence of R and ψ on wing stability, as shown in Fig. 4. When compared to Fig. 3, aft sweep of the wing to 15 deg is seen to produce a rightward shift of the divergence boundaries. Note that V_{ref} is not the same in these two figures. Figure 4 also indicates that, when compared to the wing with no sweep, a larger value of ψ is necessary to eliminate flutter from an aft-swept configuration. An additional feature of the flutter and divergence behavior, visible in Fig. 4, is that the flutter speed and divergence speed boundaries have a single common point for each value of R. However, the flutter speed and divergence

speed boundaries do not cross one another, but, instead, are tangent at this point.

Figure 5 shows the influence of stiffness cross-coupling upon flutter and divergence speed boundaries for a wing sweptback 30 deg. Stiffness cross-coupling ψ does not eliminate flutter if R is large. Even when R is small, large values of ψ are necessary to totally preclude flutter. In addition, a comparison of Figs. 3 and 5 shows that the relative positions of the dashed curves representing the divergence boundaries, as a function of R, have been reversed because of sweepback. With moderate sweepback, a low value of R (associated with high bending stiffness) appears to be disadvantageous for divergence prevention. This occurs because high bending stiffness reduces the load attenuation feature of flexible sweptback wings. Once again, note that the reference speed in Fig. 5 differs from that used in previous figures.

Figures 6 and 7 illustrate the effects of forward sweep upon stability enhancement due to tailoring. From Fig. 6, it is seen that relatively large negative values of ψ are necessary to preclude divergence of a forward-swept wing. This is particularly so if R is large. This latter difficulty is indicative of the fact that divergence tailoring relies upon bend/twist interaction. To a large extent, bending deformation is responsible for the low divergence speeds of forward-swept wings. These speeds can be increased if the wing can be tailored to twist down when the wing bends upward (and thus relieve the bending-induced aerodynamic load). This interaction will be increasingly difficult to achieve if the torsional stiffness becomes large in comparison to the bending stiffness (R is large). A similar observation was made by Niblett[5] in studies of forward-swept wing flutter and divergence.

Figure 7 reinforces these latter conclusions. In this case, the wing is swept forward 30 deg; note that it is now impossible to eliminate divergence totally when $R = 3.5$. On the other hand, flutter is nonexistent when $R = 3.5$.

These analytical results indicate that both divergence and flutter of this idealization can be eliminated for certain ranges of values of ψ. To investigate this possibility further and to determine the circumstances under which this might occur, a second study was conducted using the parameters listed in Table 1 with R fixed at 0.3. For this study, $\bar{x}_\alpha$ was allowed to take on five values: -0.20, -0.10, 0.0, 0.10, 0.20. Combinations of ψ and Λ were then determined at which flutter and/or divergence were not present.

Let us first consider divergence, and note that it is not a function of $\bar{x}_\alpha$. In Figure 8, the dashed line [computed from Eq. (32)] defines the boundary between regions in which divergence is possible and impossible. Combinations of ψ and Λ lying *below* this line are those for which divergence cannot occur because $\bar{V}_D^2$ is negative. Note the interesting tradeoff between wing sweep and stiffness cross-coupling ψ. To eliminate divergence with ψ equal to zero, this particular planform must be swept back 9.45 deg. On the other hand, if the wing is unswept, divergence can be eliminated if $\psi < -0.0913$. This illustrates the tradeoff between sweep and structural cross-coupling for static stability enhancement.

Turning to flutter, combinations of ψ and Λ lying *above* the solid lines in Fig. 9 represent totally flutter-free design. These

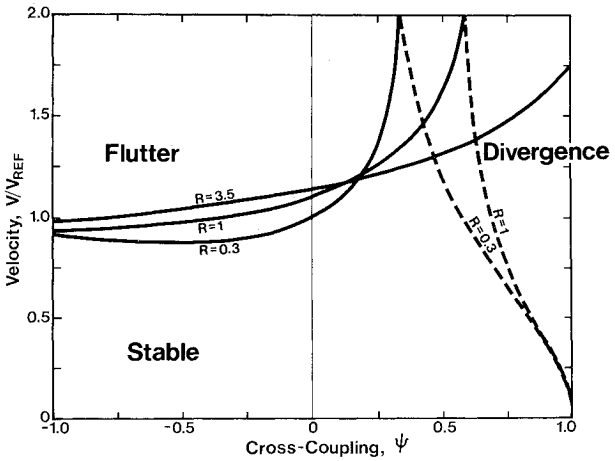

Fig. 5 Flutter and divergence speed boundaries as functions of R and ψ for a 30-deg sweptback wing; V_{ref} is unique to this sweep angle.

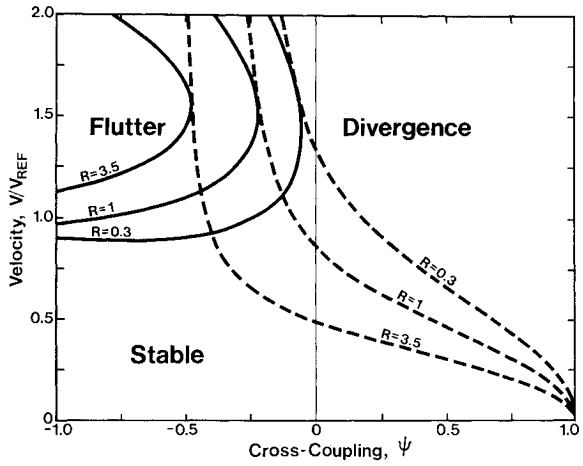

Fig. 6 Flutter and divergence speed boundaries as functions of R and ψ for a 15-deg sweptforward wing; V_{ref} is unique to this sweep angle.

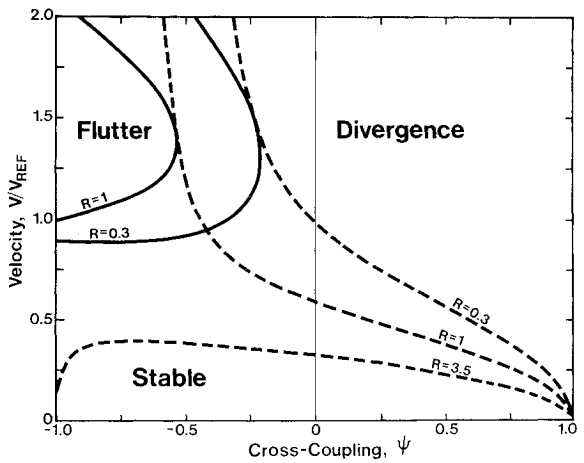

Fig. 7 Flutter and divergence speed boundaries as functions of R and ψ for a 30-deg sweptforward wing; V_{ref} is unique to this sweep angle.

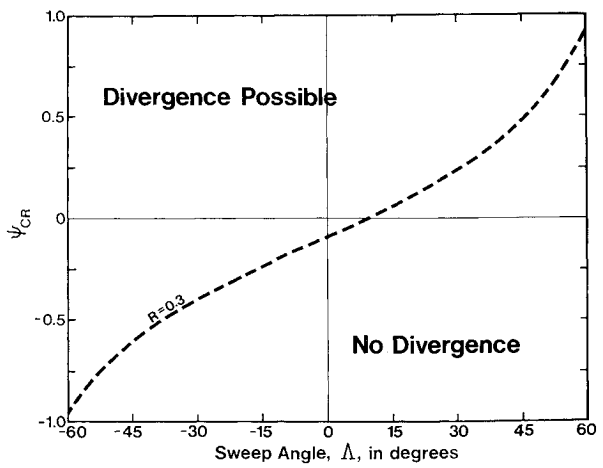

Fig. 8 Critical values of ψ and wing sweep for which the divergence speed becomes infinite. Note that although divergence is possible above the dashed line, the speed may be quite high.

lines are computed by setting the radical in Eq. (30) equal to zero and solving for ψ_{cr}. The dashed line from Fig. 8 is reproduced on Fig. 9. Note that, with $\bar{x}_\alpha = 0.20$ and $\psi = 0$, a forward sweep angle of 19.35 deg is necessary to eliminate all possibility of flutter. If wing sweep is not permitted, then a value of $\psi = 0.137$ will accomplish the same purpose.

Figure 9 indicates that aft c.g. placement ($\bar{x}_\alpha > 0$) leads to lower flutter speeds; conversely, reducing the value of $\bar{x}_\alpha$ leads to reduced requirements for structural cross-coupling. Notice that, with $\bar{x}_\alpha = 0$, this model predicts that any amount of forward sweep will eliminate flutter. This is due to the reasonably well-known fact that wing washout due to aft sweep causes a disadvantageous situation for flutter, while the wash-in tendency of a forward-swept wing has a reverse effect.

Negative static unbalance ($\bar{x}_\alpha < 0$) results in unusual, yet interesting, behavior of the flutter-free boundary. For instance, when $\bar{x}_\alpha = -0.10$ the locus of the sectional centers of mass for this example lies on the locus of the aerodynamic centers (AC) in Fig. 1c. It is well-known that a quasi-static flutter analysis of the two-dimensional typical section predicts that flutter cannot occur in such a case. This is confirmed when one examines Fig. 9 at the points $\psi = 0$, $\Lambda = 0$. However, if ψ is decreased while Λ is zero, flutter will reappear. This confirms the previous observation that wash-out behavior, whatever its source, is disadvantageous for flutter.

In Fig. 9, the boundaries associated with $\bar{x}_\alpha = 0$, -0.10, and -0.20 each consist of both curved and straight-line segments. The intersection point of these segments occurs exactly at the divergence boundary; at this point *both* flutter and divergence vanish for certain combinations of ψ, Λ, and $\bar{x}_\alpha$. This special sweep angle, denoted as Λ_{DF}, is computed from the equation

$$\tan\Lambda_{DF} = \frac{\frac{2}{3}\bar{e} + \bar{y}\bar{x}_\alpha}{2\bar{y}\bar{r}_\alpha^2 + \bar{x}_\alpha\bar{e}}\overline{R} \tag{33}$$

The value of ψ associated with this simultaneous disappearance of static and dynamic instabilities is found by substituting Eq. (33) into Eq. (32). It is interesting to note that Λ_{DF} is not a function of the primary stiffness ratio R.

For certain values of static unbalance, Fig. 9 shows that there exists a sweep angle beyond which this particular wing can be tailored to be both divergence- and flutter-free. Unless the static unbalance $\bar{x}_\alpha$ is negative, this region is likely to include only aft sweep.

Theoretically, two values of ψ_{cr} exist. Figure 9 shows the lower of these two values only. In all cases examined in these studies, the upper value of ψ_{cr} occurred outside the feasible region $-1 \le \psi \le 1$. Because of this, no upper bound to the flutter-free region was encountered. However, given the complexity of the equations discussed previously, such cases cannot be discounted entirely for other configurations.

As a final example, consider the case for which the parameters in Table 1 are fixed, but the primary stiffness ratio $R = K_{11}/K_{22}$ can take on the values $R = 0.1$, 0.3, 1.0, 2.0, and 3.0. Attention is again focused upon combinations of ψ and Λ necessary to preclude flutter or divergence. For divergence, Fig. 10 shows the effects of changes in R upon combinations of Λ, and ψ_D, the value of cross-coupling *below* which divergence is not possible. Notice that if R is small and $\psi = 0$, rather large values of aft sweep are necessary to preclude divergence. Since K_{11} is fixed, small R values are associated with large "bending" stiffness K_{22}. In such cases, the load-attenuating effect of aft-swept wing bending will be minimal. On the other hand, without wing sweep, divergence can never be eliminated without some stiffness cross-coupling, no matter how large the R ratio becomes. To see this, notice that the curve associated with $R = 3$ lies close to, but not on, the origin of Fig. 10. From Fig. 10, it appears that forward-swept wing divergence elimination is difficult (or even impossible) if R is large. For aft-swept wings, the reverse is true.

Finally, turning to flutter, Fig. 11 shows the effects of R upon the ability to control flutter of swept wings through stiffness cross-coupling. This figure indicates that flutter of a swept-forward wing is easily controlled by structural cross-coupling if ψ is allowed to be positive. In the sweptback region, large positive values of ψ are necessary to preclude flutter, especially when R is large.

How do these admittedly simplistic results compare to those generated using more sophisticated analytical models? When the cross-coupling is excluded, the trends shown for flutter and divergence boundaries appear consistent with generally accepted aeroelastic trends. To compare the present, highly idealized, results to similar, but more sophisticated, model results, an example was selected from among a group of cases involving flutter of idealized laminated wings. From these examples one was chosen that involved binary flutter as its instability mechanism.

For laminated wings, a cross-coupling parameter ψ may be defined as[6]:

$$\psi \frac{K}{\sqrt{EIGJ}} \tag{34}$$

where K is a stiffness cross-coupling parameter defined in Ref. 6. The theoretical bounds of ψ are identical to those for the previous idealization.

To analyze flutter and divergence behavior of the cantilevered laminated wing, modified strip theory utilizing two-dimensional incompressible Theodorsen aerodynamics was used together with laminated beam theory. The unswept

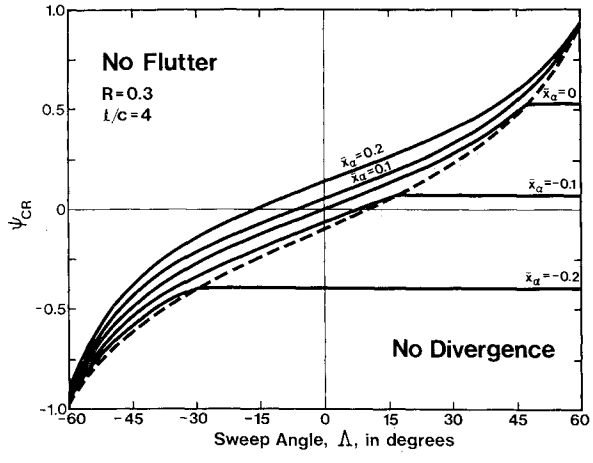

Fig. 9 Critical values of ψ and Λ for which flutter is not possible. Dashed line represents the divergence boundary from Fig. 8. Flutter will not occur for ψ,Λ combinations above the solid lines.

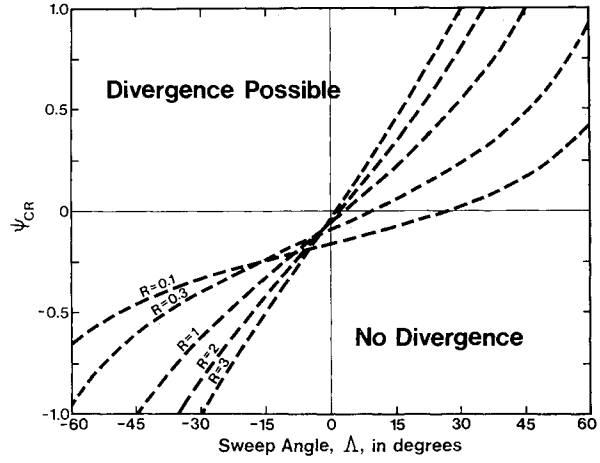

Fig. 10 Critical values of ψ and Λ for which divergence cannot occur, shown for different values of $R = K_{11}/K_{22}$.

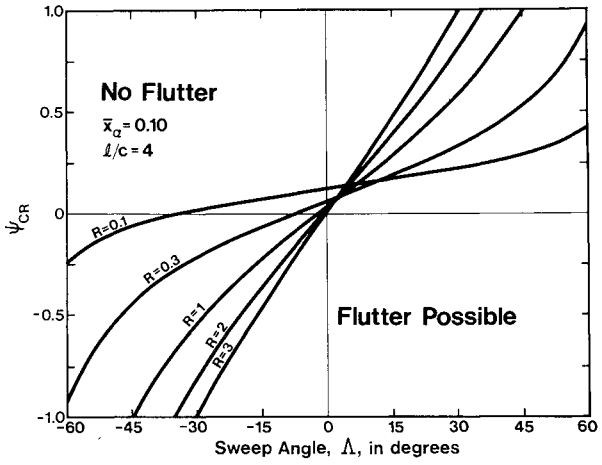

Fig. 11 Critical values of ψ and Λ for which flutter cannot occur, shown for different values of R.

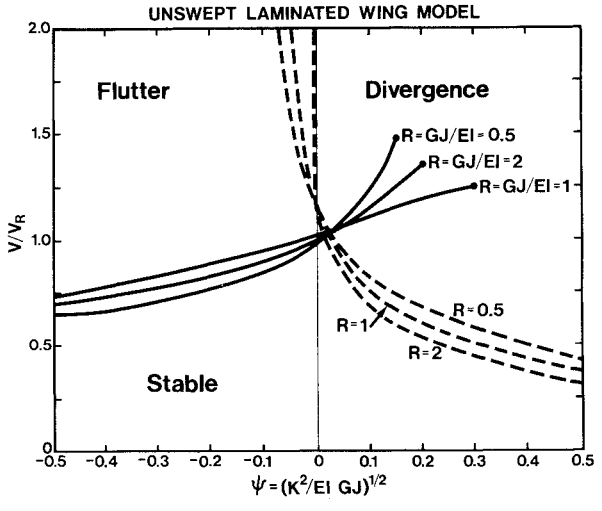

Fig. 12 Effects of beam stiffness cross-coupling ψ and $R = GJ/EI$ upon the flutter and divergence boundaries of an unswept laminated wing. V_R is the flutter speed when $R = 0.5$ and $\psi = 0$.

Table 2 Wing parameters for Fig. 12

$\ell = 160$ in.
$\bar{x}_\alpha = 0$
$\bar{r}^2_\alpha = 300$ in.^{2}
$c_{\ell_\alpha} = 6.28$/rad, a constant[a]
$c = 25$ in.
weight per length of span = 2.0 lb/in.
$GJ = 1.7 \times 10^9$ psi

[a] Reference axis is at the 35%-chord position; air density is at sea level. Two-dimensional Theodorsen aerodynamics with modified strip theory were used to generate unsteady aerodynamic loads.

laminated wing properties appear in Table 2. Three primary stiffness ratios, defined as $R = GJ/EI$, were considered in this analysis; these ratios are $R = 0.5$, 1.0, and 2.0. Results of the stability analysis are shown in Fig. 12, where nondimensional instability speed is shown plotted against the laminate cross-coupling factor ψ.

A comparison of Fig. 12 with Fig. 3 shows both similarities and differences. The flutter and divergence boundaries in both figures display the same trends. However, note that the laminated beam model has no upper flutter boundary. However, flutter may be precluded above some value of ψ. While the two-degree-of-freedom wing model does not allow penetration of the divergence boundary by the flutter boundary, flutter/divergence penetration is evident in Fig. 12.

Figure 12 indicates that larger values of ψ are required to preclude flutter when R is large. Figure 3 predicts the reverse to be true. Still, the limited comparison between the two models shows encouraging similarities. However, it must once again be cautioned that the semirigid wing model is an educational and illustrative tool, not an accurate analytical tool, as this latter comparison shows.

Conclusion

Crisp[7] presents the viewpoint that the prevention or elimination of flutter (divergence should be thought of as a special case) can be regarded as a problem in *aerodynamic balancing* rather than mass or stiffness balancing. Whether this aerodynamic balancing is done by means of inertial or structural stiffness redistribution, the result is the same. With this approach eigenfunctions (mode shapes) assume particular importance, since these mode shapes (together with reduced frequency) determine the motion-dependent air forces that act upon the structure.

Biot and Arnold[8] present a similar viewpoint in a paper that predates Crisp's. Reference 8 emphasizes the importance of the node-line position of a normal mode (they discuss a two-degree-of-freedom typical section) with respect to the ¾-chord point on the cross section. They note that the closer a node-line position lies to the ¾-chord point, the lower the flutter speed.

When ψ is negative, the node line for the first mode of the present model (usually a "bending" mode in which ϕ motion predominates) originates at the x-y origin of Fig. 1b and sweeps forward, nearly parallel to the root support. On the other hand, for negative values of ψ, the node line associated with the "torsion" mode will sweep slightly aft of the y axis (on the order of 2-4 deg) in Fig. 1b. This behavior is similar to that encountered when cross-sectional centers of gravity are placed aft of the y axis. Since aft placement of the sectional c.g. usually leads to lower flutter speeds, due to a node-line shift *aft* of the reference axis, *positive* stiffness cross-coupling can reposition the node line forward, away from the ¾-chord line "danger zone." Thus, positive cross-coupling (bend up/twist up) is equivalent to forward mass balancing in its effect on node-line position and flutter speed. A forward rotation of the structural axis ($+\gamma$) in Fig. 1b leads to negative values of ψ and enhanced divergence performance. Such rotations can place the principal stiffness direction ahead of the static aerodynamic center. As a result, the offset between the line of aerodynamic centers and a primary structural axis is decreased effectively. Conversely, the distance between the sectional centers of mass and the principal stiffness axis is increased by negative ψ, thus leading to lowered flutter speeds.

One interesting aspect of these simplified studies is the required design compromise between flutter and divergence speeds. The objective of increased flutter speed invariably leads to a wash-in (bend-up/twist-up) condition that is undesirable for divergence. Conversely, any increase in the divergence speed due to a structural wash-out (bend-up/twist-down) condition is likely to be accompanied by a lower flutter speed. The inclusion of wing sweep *and* stiffness cross-coupling as design variables leads to the possibility of further tradeoffs between aerodynamic and structural sweep. These limited results show that forward sweep of the wing causes an increase in the flutter speed and a decrease in the divergence speed. The use of tailoring to increase wing washout can achieve a harmonious balance between the flutter and divergence speeds.

Stiffness cross-coupling also appears to be aeroelastically analogous to fore or aft sweep because of the similarities between the induced wash-in/wash-out behavior. In addition, because this effect depends upon the interaction between bending and torsional deformation, the ratio of torsional to

bending stiffness R is an important parameter. From an aeroelastic optimization standpoint, one must be careful then that the objective of increasing the flutter speed does not decrease the fixed-root divergence speed to the extent that an attitude instability is triggered similar to that suffered by forward-swept wings (see Ref. 9).

Another interesting feature of this study is the theoretical finding that both flutter and divergence might be eliminated under certain special circumstances. The ability of directional stiffness to modify the vibration characteristics to the extent that the system is uncoupled or "balanced" aerodynamically is a feature worthy of further attention. Also needing attention is the development of nondimensional, bounded parameters for plate-like structures and the investigation of the extent of potential improvements in stability for various planform shapes. While the present results are based upon extreme assumptions, they nonetheless hold out promise for substantial design enhancement through judicious use of modern materials.

References

[1]Shirk, M.H., Hertz, T.J., and Weisshaar, T.A., "Aeroelastic Tailoring—Theory, Practice, Promise," *Journal of Aircraft*, Vol. 23, Jan. 1985, pp. 6-18.

[2]Bisplinghoff, R.L., Ashley, H., and Halfman, R.L., *Aeroelasticity*, Addison-Wesley, Reading, MA, 1956, pp. 527-545.

[3]Diederich, F.W., *AGARD Manual on Aeroelasticity*, Pt. III, Nov. 1963, Chap. 3.

[4]Hermann, G., "Dynamics and Stability of Mechanical Systems with Follower Forces," NASA CR-1782, Nov. 1971.

[5]Niblett, L.T., "Divergence and Flutter of Swept-Forward Wings with Cross-Flexibilities," Royal Aircraft Establishment TR 80047, April 1980.

[6]Weisshaar, T.A. and Foist, B.L., "Vibration Tailoring of Advanced Composite Lifting Surfaces," *Journal of Aircraft*, Vol. 22, Feb. 1985, pp. 141-147.

[7]Crisp, J.D.C., "The Equation of Energy Balance for Fluttering Systems with Some Applications in the Supersonic Regime," *Journal of the Aerospace Sciences*, Nov. 1959, pp. 703-716, 738.

[8]Biot, M.A. and Arnold, L., "Low-Speed Flutter and Its Physical Interpretation," *Journal of the Aeronautical Sciences*, April 1948, pp. 232-236.

[9]Weisshaar, T.A. and Zeiler, T.A., "Dynamic Stability of Flexible Forward Swept Wing Aircraft," *Journal of Aircraft*, Vol. 20, Dec. 1983, pp. 1014-1020.